Selected Papers

Catalytic Hydrogenation of Carbon Dioxide with a Highly Active Hydride on Ir(III)–Pincer Complex: Mechanism for CO_2 Insertion and Nature of Metal–Hydride Bond

Jun Li[1] **and Kazunari Yoshizawa***[1,2]

[1]Institute for Materials Chemistry and Engineering, Kyushu University, Fukuoka 819-0395

[2]International Research Center for Molecular Systems, Kyushu University, Fukuoka 819-0395

Received May 9, 2011; E-mail: kazunari@ms.ifoc.kyushu-u.ac.jp

A reaction mechanism for the hydrogenation of CO_2 to formate catalyzed by an Ir(III)–pincer trihydride complex has been investigated with density functional theory calculations. Two routes for the formation of formate were considered: (I) the insertion of CO_2 into the Ir–H bond with the assistance of the metal center, and (II) the direct addition of hydride to CO_2 via nucleophilic attack. Route II is energetically more favorable than route I. Molecular orbital and natural bond orbital analyses showed that this trihydride complex consists of two kinds of hydrides with distinct Ir–H bond properties, and the hydride in the plane vertical to the pyridine moiety is highly active. The whole catalytic cycle for CO_2 hydrogenation to formate is exothermic by 30.3 kcal mol^{-1}, and the rate-limiting step is the regeneration of the active complex, which involves a barrier of 15.6 kcal mol^{-1}. The theoretical results are in good agreement with and give a reasonable explanation to the experimental observations. Moreover, the results imply that the type of a metal–hydride bond might determine which route the CO_2 insertion takes, route I or route II.

The capture and fixation of carbon dioxide, a greenhouse gas, has attracted dramatically increasing attention, due to its contribution to global warming. As an abundant C1 source, CO_2 can be used to synthesize many value-added organic compounds.[1–5] Hydrogenation of CO_2 to produce formic acid is one of these interesting subjects of research. Formic acid is an important product that can be used as a preservative and an insecticide in usual applications, and as an acid, a reductant, and a carbon source in chemical synthesis.[6] Catalytic hydrogenation of CO_2 has been widely studied by using transition-metal complexes,[1,7] especially based on rhodium,[8] ruthenium,[9] and iridium.[10] Recently, Nozaki and co-workers reported a highly active catalyst for the hydrogenation of CO_2 (Scheme 1).[11] Treatment of an iridium(III)–pincer trihydride complex ([IrPNPH$_3$], PNP: 2,6-(diisopropylphosphinomethyl)-pyridine) with CO_2 led to an immediate equilibrium between the trihydride and a dihydrido formate at room temperature. The highest turnover numbers (TON) reached up to 3.5 million. Exposure of the formate in aqueous KOH to H_2 resulted in the elimination of formate anion and the regeneration of the starting [IrPNPH$_3$] complex.

Hydrogenation of CO_2 has been theoretically investigated with several transition-metal complexes as catalyst.[12–20] Two routes were proposed for the insertion of CO_2 into a metal–hydride bond: (I) through the precoordination of CO_2 to the metal center followed by hydride migration to CO_2, shown as route I in Scheme 2; (II) via the direct addition of hydride to CO_2 and the subsequent rotation of the formato ligand, shown as route II. Most work has supported route I because in it

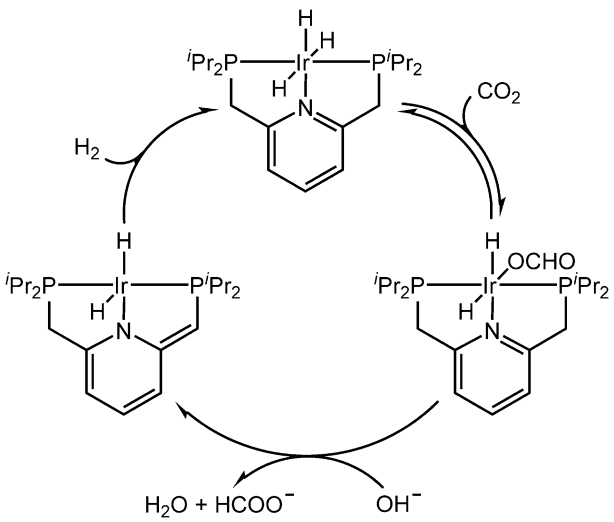

Scheme 1. Proposed catalytic cycle for the hydrogenation of CO_2 to formate.[11]

the cooperation of the metal center is involved when CO_2 is inserted into the metal–hydride bond. Only a few examples favoring route II were reported by Matsubara,[17,18] Sakaki and co-workers,[19] and Baiker and co-workers.[20] For example, Matsubara reported that the direct hydride addition to CO_2 is favorable in the hydrogenation of CO_2 to formic acid on a Ru complex and indicated that route II is preferred in his example because the promotion effect of the protonated amine arm is only effective for route II.[17]

Published on the web October 6, 2011; doi:10.1246/bcsj.20110128

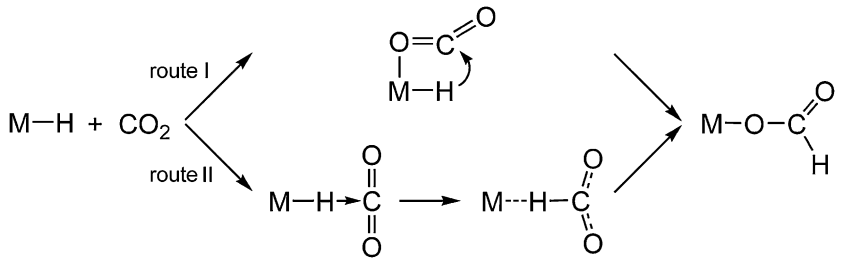

Scheme 2. Two mechanisms for CO_2 insertion into the metal–hydride bond.

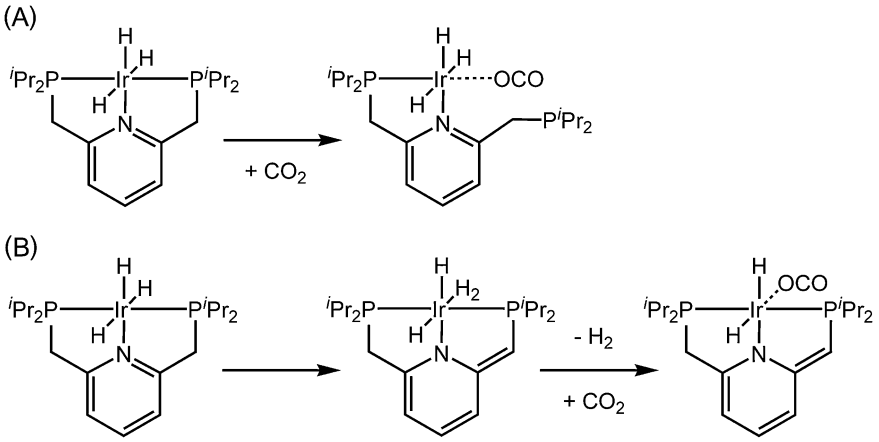

Scheme 3. Two possible methods for the coordination of CO_2 to the metal center.

In this study we would like to examine these two routes for the insertion of CO_2 into the Ir–H bond of the [IrPNPH$_3$] complex and then explore the pathways for the elimination of formate anion and the regeneration of the starting active complex with density functional theory (DFT) calculations. Ahlquist suggested a two-step mechanism (route II) for the formation of formate based on DFT calculations with a simplified model (the isopropyl groups were replaced by two H atoms).[21] In the present work a full model (the real active complex) was adopted and the geometries of all species were optimized in aqueous phase in order to take into account the steric effects and the solvent effects. Furthermore, molecular orbital (MO) and natural bond orbital (NBO) analyses were made to understand the mechanism for the direct addition of hydride to CO_2 and the nature of the Ir–H bonds in the [IrPNPH$_3$] complex. Moreover, on the basis of the calculations performed in aqueous phase, we suggested an alternative pathway for the regeneration of the [IrPNPH$_3$] complex that is more compatible with the experimental observations.

Computational Methods

All calculations were performed with the Gaussian 09 program.[22] The B3LYP hybrid functional[23] was used. For iridium the Stuttgart–Dresden basis set-relativistic effective core potential (RECP) combination[24] was applied and the Stuttgart–Dresden basis set was supplemented with two sets of *f* functions and a set of *g* functions.[25] For P, O, N, C, and H atoms, the Dunning cc-pVDZ basis set[26] was applied for geometry optimizations and frequency calculations; and the aug-cc-pVDZ basis set[27] with diffuse functions was applied for single point energy corrections. All calculations were carried out in aqueous phase. The solvent effects were approximated using polarizable continuum model (PCM),[28] specially the integral equation formalism model (IEF-PCM).[29] Each stationary point was confirmed as minimum or transition state from the vibrational frequency. In addition, all the transition states were verified by intrinsic reaction coordinate (IRC) calculations. The bond properties were characterized by natural bond orbital (NBO) analysis.[30] The heterolytic dissociation energy of the Ir–H bond was calculated as: $E = E(H^-) + E(L_nIr^+) - E(L_nIr\text{–}H)]$. $E(L_nIr\text{–}H)$ is the single point energy at the aug-cc-pVDZ level of the [IrPNPH$_3$] complex whose geometry is optimized at the cc-pVDZ level, and $E(L_nIr^+)$ is the single point energy at the aug-cc-pVDZ level of the moiety with hydride removal from the optimized IrPNPH$_3$ complex.

Results and Discussion

CO_2 Insertion into the Ir–H Bond. The Ir(III)–pincer trihydride complex ([IrPNPH$_3$]) takes an octahedral geometry with the metal center hexacoordinated, which blocks the approach of CO_2 to Ir. In some reactions involving transition-metal complexes with the PNP or PNN ligand, the metal–P or metal–N linkage can be opened for the coming of the reactive molecules to the metal center.[31,32] Thus, we considered a possible method for the coordination of CO_2 to Ir, in company with the Ir–P linkage cleavage, shown as method (A) in Scheme 3. Moreover, some experimental work reported that H_2 was released from some transition-metal–PNP (or PNN) complexes.[33–35] Our previous work also theoretically demonstrated that the release of H_2 from a Ru(II)–PNN hydrido–hydroxo complex is possible.[36] On this account, we considered another possible method in that CO_2 will be coordinated at the vacant site released by H_2 (method (B)). However, these two methods for CO_2 coordination to Ir were both found to be

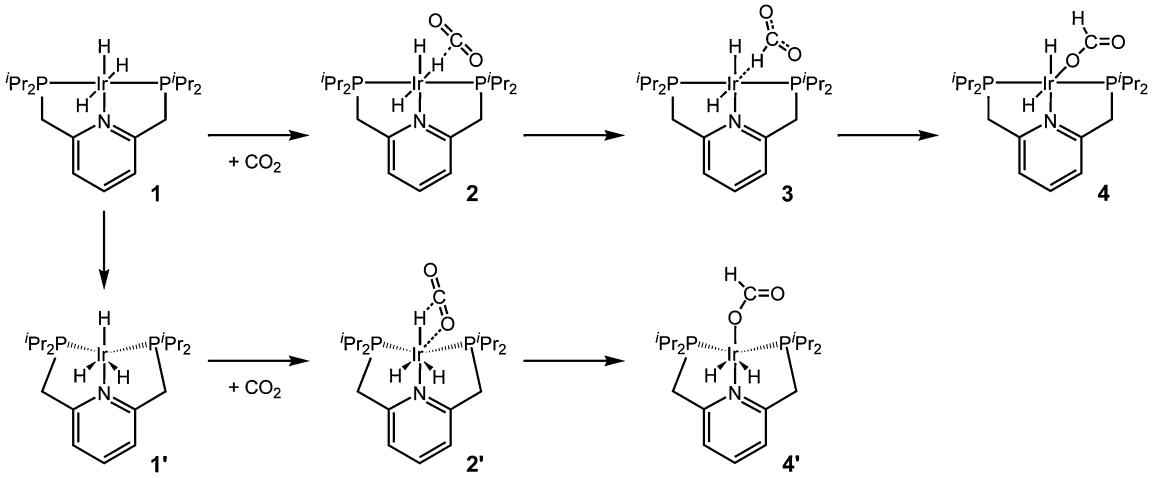

Scheme 4. Two possible pathways for the insertion of CO_2 into the Ir–H bond of the [IrPNPH$_3$] complex **1** to form formate.

energetically unfavorable. Method (A) is endothermic by 38.6 kcal mol^{-1}, due to the very weak interaction of CO_2 with the metal center. Method (B) is endothermic by 18.3 kcal mol^{-1} and has a high activation barrier of 35.5 kcal mol^{-1}, which is in agreement with the release of H_2 being not mentioned in the experimental paper.[11] The detailed geometries and energies of all species involved in these two pathways are provided in the Supporting Information.

We then thought about the possibility of the direct addition of hydride to CO_2 without the help of the metal center. The proposed pathway is illustrated in Scheme 4. First, CO_2 interacts with the active complex **1** to form a precursor complex **2**, which will lead to the formation of an H-bound formate complex **3** via nucleophilic attack of the hydride to CO_2. Subsequently, the rearrangement of **3** yields an O-bound formate complex **4**. It is interesting that we came across an isomer of **1**, namely **1′**, which takes a quasi-octahedral geometry. In **1** all the H–Ir–P angles are nearly 90.0° so that the approach of CO_2 to Ir will be hindered; but in **1′** there is a P–Ir–P angle of 120.1° that is beneficial for the approach of CO_2 to Ir. After CO_2 approaches **1′**, the association complex **2′** will not result in the direct hydride addition to CO_2, as occurs on **2**. With the assistance of the metal center, CO_2 is inserted into the Ir–H bond and the O-bound formate complex **4′** is formed. Note that in **4′** the formato ligand is located *cis* to both hydrido ligands, whereas in **4** the formato ligand is located *cis* to one hydrido ligand and *trans* to the other. We will discuss these two pathways for CO_2 insertion into the Ir–H bond to form formate in detail. The energy diagrams for these two pathways are shown in Figure 1, and the optimized geometries of all species involved are presented in Figures 2 and 3.

The formation of the formate **4** via the direct addition of hydride to CO_2 includes three steps. At first, the interaction of CO_2 with the trihydride complex **1** gives the precursor complex **2** with an energy change of 2.3 kcal mol^{-1}. The angle of O–C–O in **2** is 178.9°, slightly bent from the angle of the linear CO_2 molecule, because CO_2 is weakly hydrogen-bonded with the surrounding methyl groups. The total natural charge of CO_2 in **2** is 0.005. Second, the hydride directly migrates to CO_2 via nucleophilic attack, leading to the H-bound formate complex **3**. This step is endothermic by 0.4 kcal mol^{-1} and has a very low activation barrier of 4.2 kcal mol^{-1}. In **3** the O–C–O angle is bent (136.7°) and the total natural charge of the CO_2 moiety falls to −0.655, indicating that electrons have been transferred into CO_2 and the formate is formed. The CO_2 moiety is stabilized by more and stronger hydrogen bonds. But **3** is not a stable intermediate since the relative energy of **3** is above **1** + CO_2. It should be noticed that the Ir–H bond involved in the reaction has been greatly weakened (from 1.678 Å in **2** to 1.846 Å in **3**), while the Ir–H bond on the other side is strengthened (from 1.687 to 1.590 Å). Finally, **3** rearranges itself to form the O-bound formate complex **4** through the rotation of the formato ligand. This step is exothermic by 6.7 kcal mol^{-1} and has an activation barrier of 8.3 kcal mol^{-1}. In this step the Ir–H bond is completely cleaved and CO_2 is inserted into the Ir–H bond. The distance of the C–H bond in the formato ligand is greatly shortened from 1.252 Å in **3** to 1.123 Å in **4**, very close to the distance of the C–H bond in formic acid (1.108 Å). The overall process is slightly exothermic by 4.0 kcal mol^{-1} and the highest barrier on the potential energy surface is 11.0 kcal mol^{-1} with respect to **1** + CO_2. This result is in good agreement with the result obtained by Ahlquists that this reaction is exothermic by 8.3 kcal mol^{-1} and has a barrier of 10.8 kcal mol^{-1}.[21] A low barrier for the direct addition of hydride to CO_2 was also reported for some other transition-metal complexes. For example, Baiker and co-workers published that the insertion of CO_2 into a Ru–H bond of the complex [$(PMe_2CH_2CH_2PMe_2)_2RuH_2$] involves a barrier of 17.4 kcal mol^{-1} for a *cis*-route and 7.8 kcal mol^{-1} for a *trans*-route.[20] The calculated energies for this pathway indicate that it is facile and reversible, in accordance with the experimental observation that the reaction of **1** with CO_2 led to an immediate equilibrium between **1** and a dihydrido formate.[11]

The starting point of another possible pathway for the formation of formate is **1′**, being 6.7 kcal mol^{-1} above its isomer **1**. The barrier for the isomerization of **1** to **1′** is 27.7 kcal mol^{-1}. Different from **1**, **1′** takes a quasi-octahedral geometry and has a relatively large P–Ir–P angle (120.1°), due to the strong repulsion between two big isopropyl groups. The larger P–Ir–P angle in **1′** is beneficial for the approach of CO_2 to Ir to form the association complex **2′**. The formation of **2′** is endothermic by 2.3 kcal mol^{-1}, indicating that **2′** is not stable.

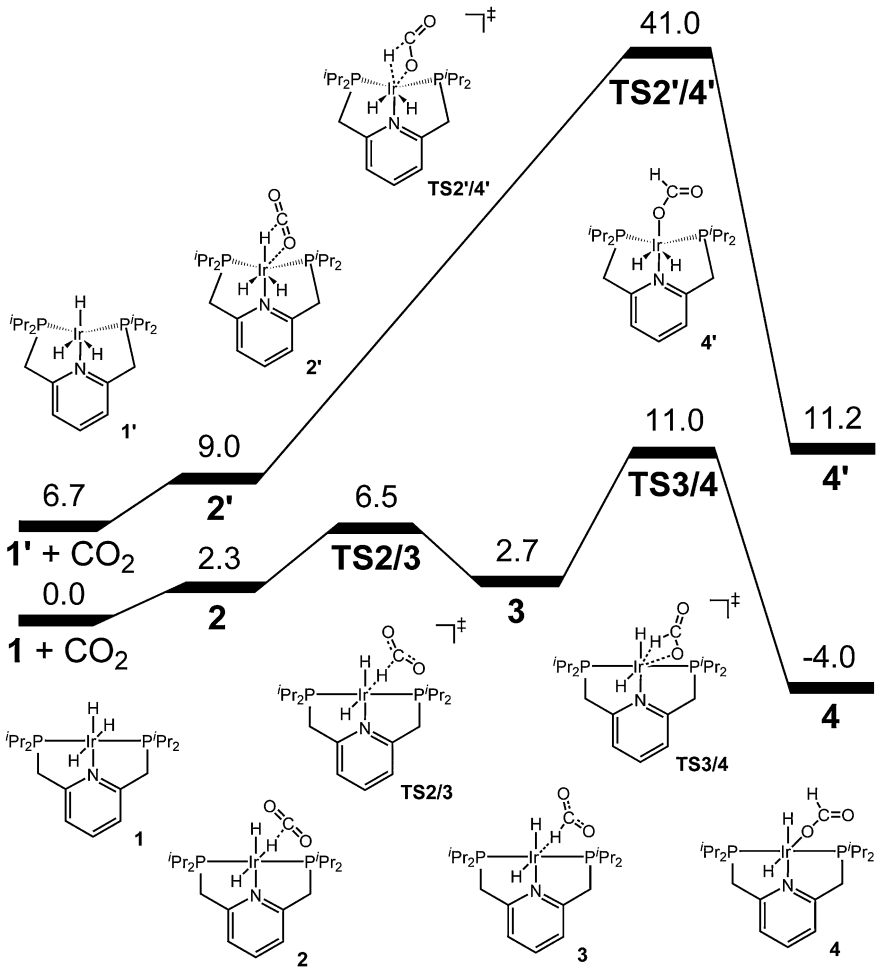

Figure 1. Energy diagrams for the insertion of CO_2 into the Ir–H bond of **1** to form formate (ΔE, in kcal mol^{-1}). Corrections for zero-point vibrational energies were made.

The angle of O–C–O in **2′** is 179.3° and the total natural charge of CO_2 moiety is 0.007. The hydride bonding with CO_2 in **2′** cannot directly migrate to CO_2, as occurs on **2**. But CO_2 might be inserted into the Ir–H bond with the assistance of the metal center. The intermediate derived is the O-bound formate complex **4′**, which is formed via a four-member ring transition state **TS2′/4′**. In this transition state the migration of hydride to CO_2 is in concert with the coordination of CO_2 to Ir. Nevertheless, this step has an activation barrier as high as 32.0 kcal mol^{-1}, being endothermic by 2.2 kcal mol^{-1}. As a whole, this pathway is not favorable in comparison with the previous pathway. Nozaki and co-workers reported that the obtained formate complex shows two distinct hydride signals.[11] It indicates that the formate obtained in the experiment should be **4** instead of **4′**. It is notable that the direct addition of hydride to CO_2 via nucleophilic attack is so facile, whereas the insertion of CO_2 into the Ir–H bond with the cooperation of the metal center is so unfavorable. Although there have been some examples favoring the insertion of CO_2 into a metal–hydride bond via direct hydride addition, this is the first example in that the active complex consists of two kinds of hydrides: One is involved in route I and the other in route II; more importantly, route I is much less favorable than route II. This example provides us useful insight into why some metal–hydride bonds can achieve the direct addition of hydride to CO_2 and some cannot. To this end, we performed MO and NBO analyses of **1** and **1′** and will discuss in detail later.

Elimination of Formate Anion and the Regeneration of the Active Complex. After formate is produced, the elimination of formic acid often takes place.[14–16] In this case two possible routes contribute to the elimination of formic acid, as shown in Scheme 5: (a) reductive elimination via proton capture from the neighboring hydrido ligand, accompanied with the reduction of the metal center to Ir(I); (b) nonreductive elimination via proton transfer from the side arm to the formato ligand, in company with the dearomatization of the pyridine ring. However, the reductive elimination of formic acid is calculated to be endothermic by 26.1 kcal mol^{-1} and the latter is endothermic by 30.0 kcal mol^{-1}. As a result, the elimination of formic acid from **4** is thermodynamically unfeasible.

But the substitution of the formato ligand by the hydroxy group is available. The proposed pathway for the elimination of formate anion is shown in Scheme 6 and the potential energy changes of this pathway is presented in Figure 4. The elimination of formate anion from **4** gives a cationic dihydride complex **5**, with an energy change of 7.9 kcal mol^{-1}. The reassociation of **5** with the OH group stabilizes **5** by 20.2 kcal mol^{-1}, resulting in the dihydrido–hydroxo complex **6**.

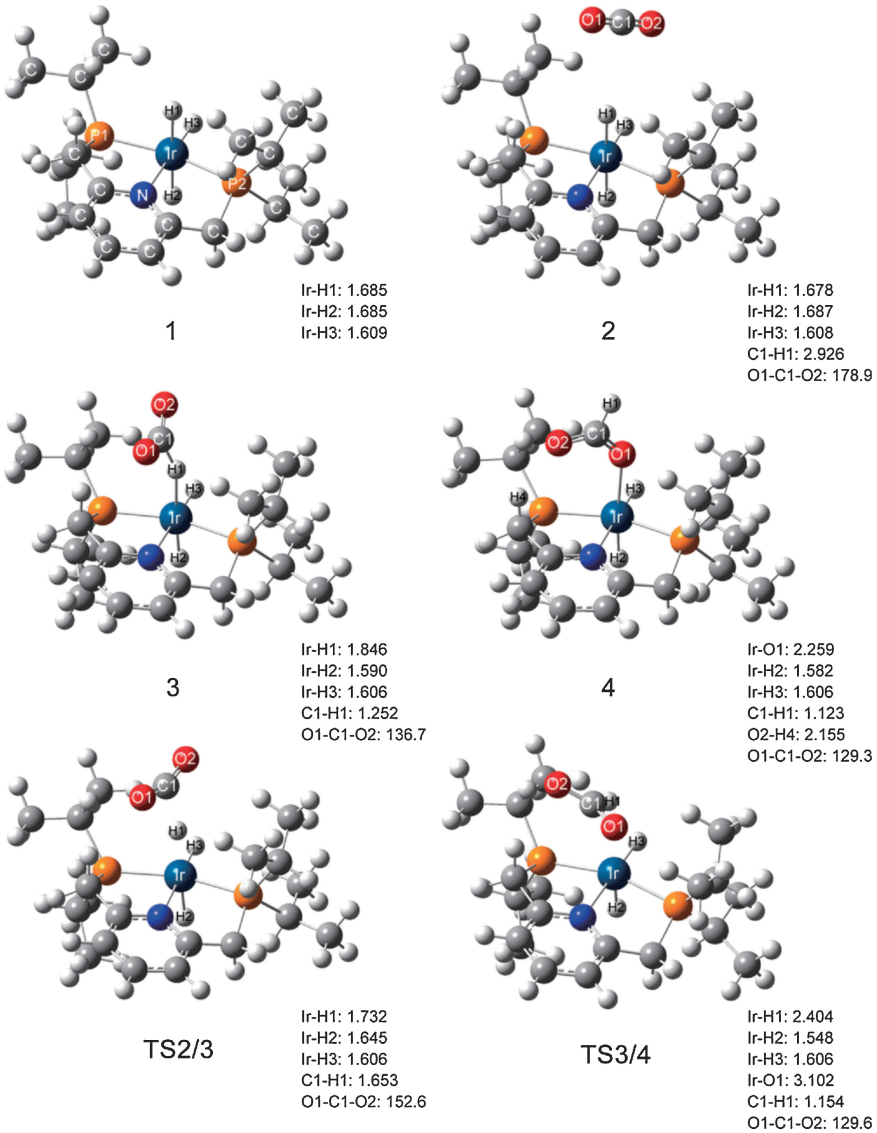

Figure 2. Optimized geometries of all species involved in the direct hydride addition to CO_2 to form formate **4**. Bond distances are in angstrom (Å) and bond angles are in degree (°). Selected natural charges (in electron, e) on **1**: Ir: −0.177, H1: −0.307, H2: −0.307, H3: −0.119; on **2**: Ir: −0.179, H1: −0.300, H2: −0.313, H3: −0.117, C1: 1.087, O1: −0.542, O2: −0.540; on **3**: Ir: −0.148, H1: −0.070, H2: −0.025, H3: −0.112, C1: 0.773, O1: −0.718, O2: −0.710.

The optimized geometries of **5** and **6** are provided in the Supporting Information.

We previously investigated a similar hydrido–hydroxo complex with PNN pincer ligand and found that proton transfer can proceed easily and reversibly between the side arm and the hydroxo (or hydrido) ligand to form or split H_2O and H_2.[36] This process proceeds under the cooperation of the metal center and the pincer ligand that can be dearomatized and rearomatized. Here a similar mechanism is suggested for the subsequent reactions on **6**, as shown in Scheme 7. The formation of H_2O on **6**, the substitution of H_2O by H_2, and the dissociation of H_2 regenerate the starting trihydride complex **1**. The relative energies of all species involved in the three steps are given in Figure 4. The optimized geometries of these species are provided in the Supporting Information.

First, an aquo complex **7** will be formed with the deprotonative dearomatization of the pincer ligand. A proton migrates from the side arm to the hydroxo ligand, leading to the formation of H_2O. The metal center remains as Ir(III). This step is endothermic by 11.6 kcal mol^{-1} and has an activation barrier of 14.1 kcal mol^{-1}. Next, H_2O will be replaced by H_2. The release of H_2O from **7** is endothermic by 0.5 kcal mol^{-1}, while the coordination of H_2 to the resulting complex **8** is exothermic by 7.8 kcal mol^{-1}. As a result, a dihyhrogen complex **9** is formed. Finally, H_2 will be heterolytically broken by the cooperation of the metal center and the side arm, in which the pincer ligand is aromatized and the starting active complex **1** is produced. This step is exothermic by 18.3 kcal mol^{-1} and involves a moderate activation barrier of 17.2 kcal mol^{-1}. In addition, water molecule can facilitate the dissociation of H_2 on **9**. Water acts as a bridge of proton transfer that donors a proton to the dearomatized pincer ligand, and at the same time accepts a proton from the coordinating H_2 (**10** → **11**). The barrier for the dissociation of H_2 is decreased to 15.6 kcal mol^{-1} relative to **10**.

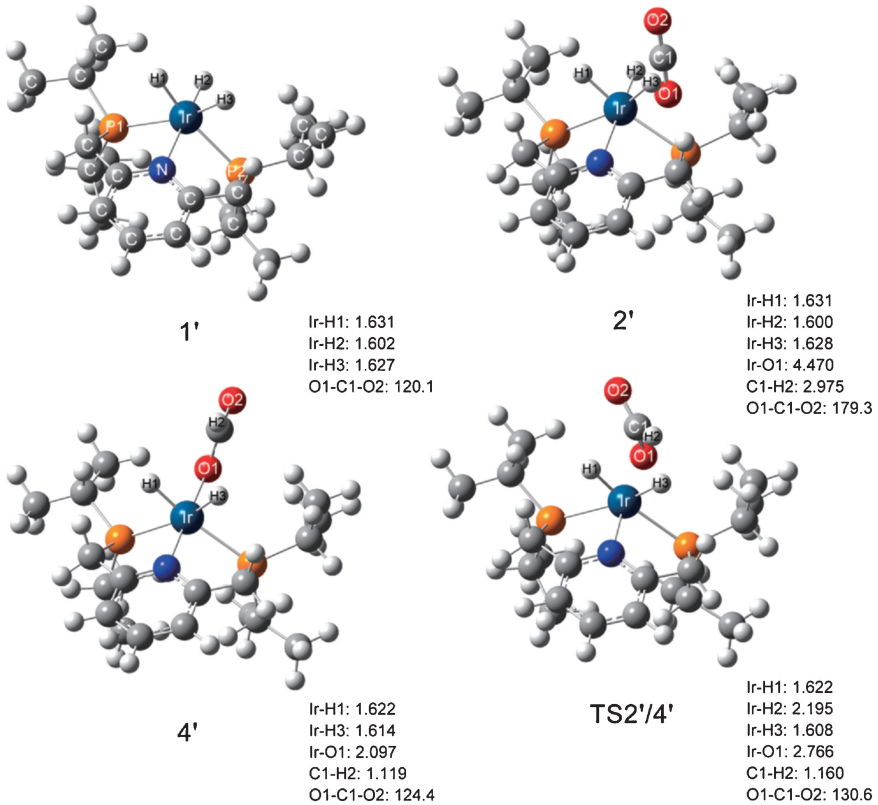

Figure 3. Optimized geometries of all species involved in the formation of formate **4′** with the assistance of the metal center. Bond distances are in angstrom (Å) and bond angles are in degree (°).

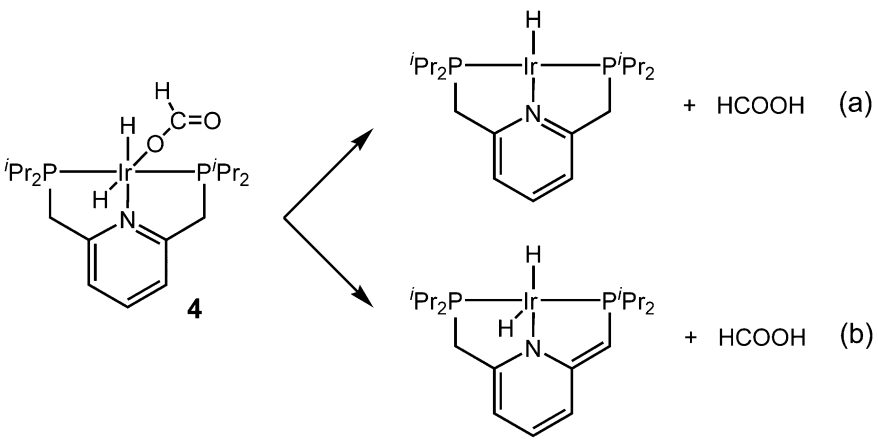

Scheme 5. Two possible routes for the elimination of formic acid.

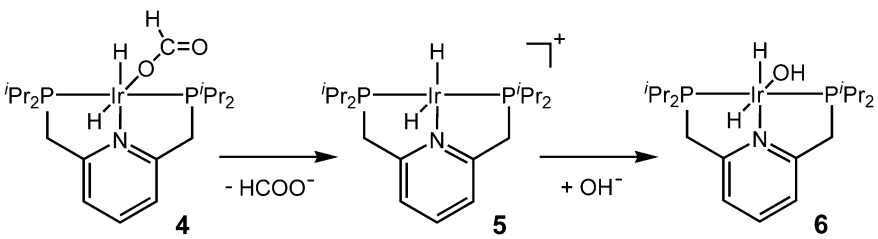

Scheme 6. Proposed pathway for the elimination of formate anion.

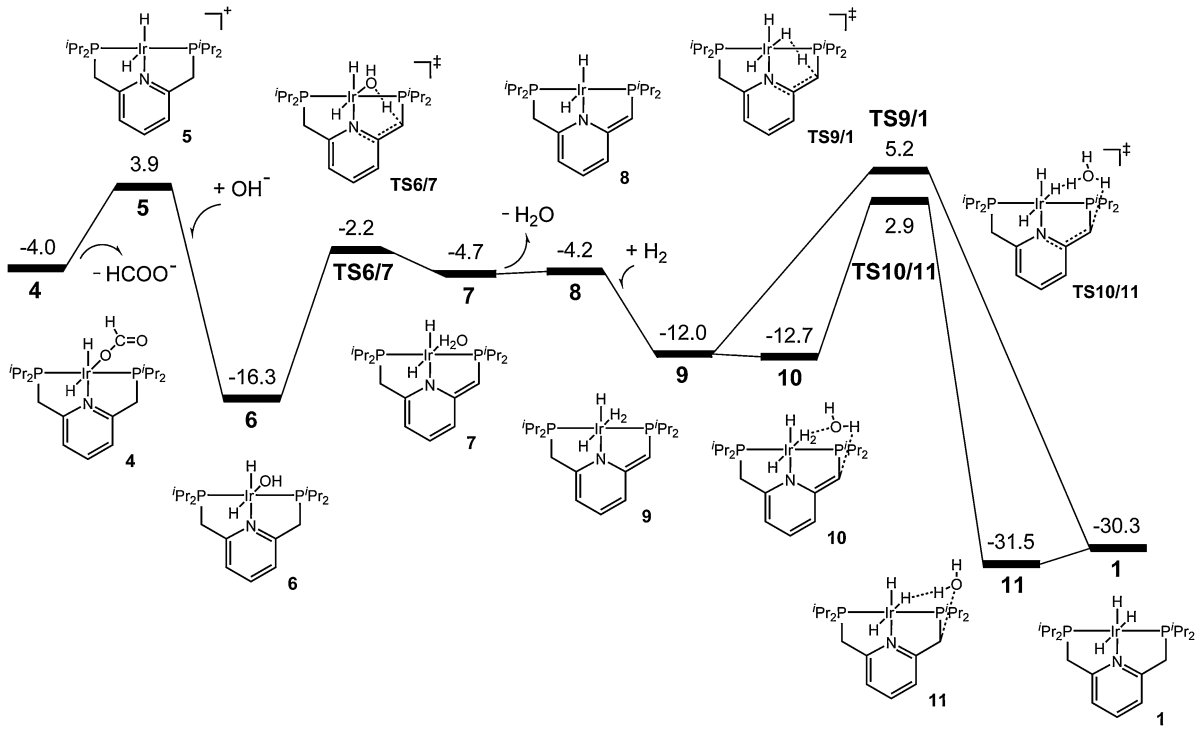

Figure 4. Energy diagram for the elimination of formate anion and the regeneration of the active complex **1** (ΔE, in kcal mol^{-1}). Corrections for zero-point vibrational energies were made.

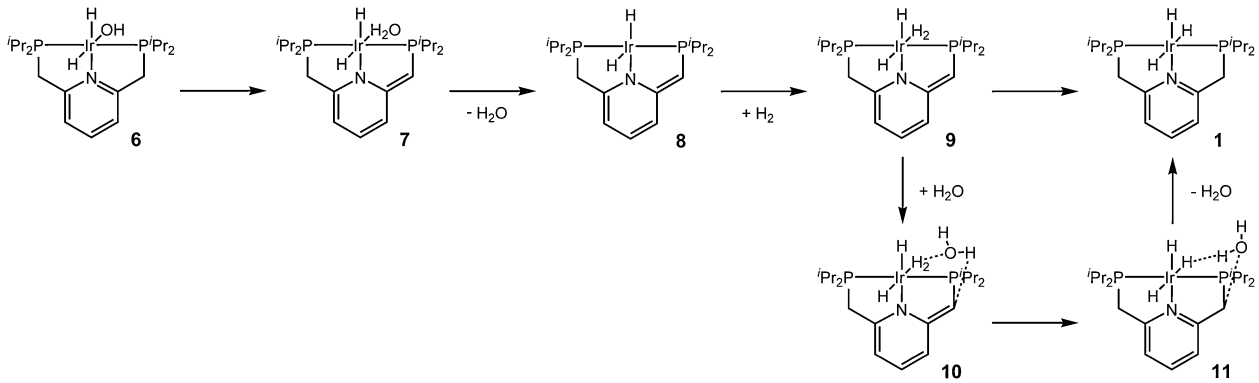

Scheme 7. Proposed pathway for the regeneration of the active complex **1**.

Ahlquist reported that the geometry of the dihydride complex **8** is trigonal bipyramidal rather than square pyramidal.[21] In this study we found that **8** with a trigonal-bipyramidal geometry is 2.1 kcal mol^{-1} higher in energy when the geometries are optimized in aqueous phase, which is in accord with the experimental result that a square-pyramidal **8** was synthesized.[11] Ahlquist suggested that for the regeneration of **1**, a key step is the formation of a cationic [Ir(H)$_2$(H$_2$)] complex via H$_2$ coordination to **5**.[21] He reported that this process is exothermic by 10.7 kcal mol^{-1}. In this study we calculated it to be exothermic by 6.6 kcal mol^{-1}. As mentioned above, the coordination of OH group to **5** is exothermic by 20.2 kcal mol^{-1}. As a result, the coordination of OH group to **5** is preferred and the formation of the cationic [Ir(H)$_2$(H$_2$)] complex is suppressed.

CO$_2$ insertion into **1** to form formate, formate anion elimination when the base exists, H$_2$O formation with the dearomatization of the pincer ligand, and H$_2$ dissociation to rearomatize the pincer ligand and regenerate **1** complete the catalytic cycle (Schemes 4, 6, and 7). The whole cycle is exothermic by 30.3 kcal mol^{-1}. The formation of **4** is slightly exothermic by 4.0 kcal mol^{-1} and has a low barrier of 11.0 kcal mol^{-1}, indicating that the formation of formate is facile and reversible. The regeneration of the active complex **1** has the highest activation barrier (15.6 kcal mol^{-1}), being the rate-limiting step. All the results obtained in this study are in good agreement with and give a reasonable explanation for the experimental observations.[11]

MO and NBO Analyses of the IrPNPH$_3$ Complex. As mentioned above, there exist two routes for the insertion of CO$_2$ into a metal–hydride bond: (I) Hydride migration to CO$_2$ after CO$_2$ coordination to the metal center, (II) direct hydride addition to CO$_2$ without the assistance of the metal center. Route I occurs with the concerted cooperation of the metal

Table 1. Bond Distances, Stretching Frequencies, and Dissociation Energies of the Ir–H Bonds in **1** and **1′**

	1		**1′**
	Ir–H1	Ir–H3	Ir–H2
Distance/Å	1.685	1.609	1.602
Stretching frequency/cm^{-1}	1635.8	2126.9	2156.9
Dissociation energy[a]/kcal mol^{-1}	51.5	78.6	79.3

a) Heterolytic dissociation of Ir–H bond: $L_nIr–H \rightarrow L_nIr^+ + H^-$. L represents the ligands coordinated to Ir, and n is the number of the ligands.

Table 2. Orbital Energies, Occupancies, and Compositions of the Ir–H Bonds in **1** and **1′**

	Type	Energy /a.u.	Occupancy /e	Coefficients/Hybrids
1 Ir–H1	σ	0.168	0.941	0.732 H(s) + 0.681 Ir($sd^{1.73}$)
	σ^*	1.078	0.316	−0.681 H(s) + 0.732 Ir($sd^{1.73}$)
Ir–H3	σ	0.233	0.961	0.712 H(s) + 0.702 Ir($sd^{2.69}$)
	σ^*	0.951	0.143	−0.702 H(s) + 0.712 Ir($sd^{2.69}$)
1′ Ir–H2	σ	0.250	0.963	0.709 H(s) + 0.705 Ir($sd^{2.69}$)
	σ^*	0.825	0.140	−0.705 H(s) + 0.709 Ir($sd^{2.69}$)

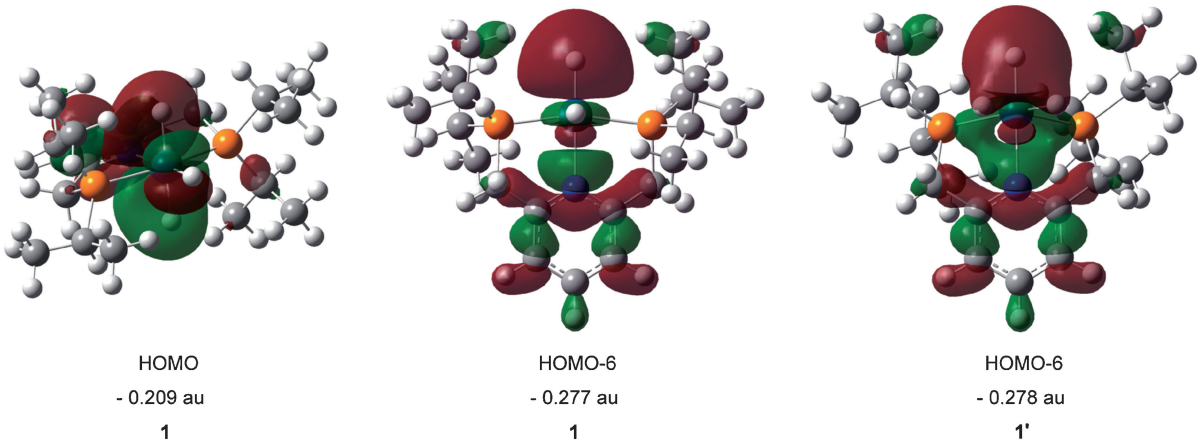

Figure 5. Selected molecular orbitals in the active complex **1** and **1′**.

center and route II functions just via nucleophilic attack. As a result, route I is preferred in more cases. However, in this case route II is more favorable than route I. The [IrPNPH$_3$] complex consists of one hydride that is involved in route I and another hydride that is involved in route II. This complex provides us with a chance to understand which hydride has sufficient activity for the direct addition to CO_2.

We collected some characteristics of the Ir–H bonds of **1** and **1′** in Table 1. The Ir–H1 bond of **1** can accomplish the direct addition of hydride to CO_2 and the Ir–H2 bond of **1′** cannot. The distances, stretching frequencies, and dissociation energies of the Ir–H1 bond of **1** and the Ir–H2 bond of **1′** show that these two Ir–H bonds are very different. The longer distance and smaller stretching frequency of the Ir–H1 bond in **1** indicate that it is weaker. If the hydride on the Ir–H1 bond of **1** is dissociated, an energy of 51.5 kcal mol^{-1} will be required. For the hydride dissociation from the Ir–H2 bond in **1′**, an energy of 79.3 kcal mol^{-1} should be compensated. The difference between these two dissociation energies is close to the difference between the energies of **TS3/4** and **TS2′/4′**. All these characteristics indicate that the hydride on the Ir–H1 bond of **1** is more active. Note that the Ir–H3 bond of **1** has similar characteristics to the Ir–H2 bond of **1′**. Another thing in common for the two Ir–H bonds is that they are both in the plane of the pyridine moiety. But the Ir–H1 bond of **1** is vertical to the plane of the pyridine moiety.

We next examined the molecular orbitals of **1** and **1′** to find out why the hydride on the Ir–H1 bond of **1** is so active that it can attack CO_2 directly. As shown in Figure 5, the highest occupied molecular orbital (HOMO) of **1** represents the bonding combinations of the Ir orbitals with the orbital of the hydride H1. However, the mixing of the Ir orbitals with the orbital of the hydride H2 in **1′**, and with the orbital of the hydride H3 in **1** constructs the HOMO−6 orbital in **1′** and **1**, respectively. As a result, when CO_2 is attacked by the hydride H1, the HOMO of **1** can overlap with the π^* orbital of CO_2 in a bonding way, considerably increasing the negative charges on the O atoms of CO_2. A similar mechanism for the nucleophilic attack of a hydride to CO_2 was also suggested on a Ru complex.[19]

NBO analysis was further performed to make clear the nature of the Ir–H bonds in **1** and **1′**. The bonding information for the Ir–H1 bond and the Ir–H3 bond in **1**, and the Ir–H2 bond in **1′** is collected in Table 2. The Ir–H1 bond in **1** is a σ bond formed from the mixing of the 1s orbital of hydride with the $sd^{1.73}$ hybrid orbital of Ir. The Ir–H3 bond in **1** and the Ir–H2 bond in **1′** are both constructed via the mixing of the 1s orbital of hydride with the $sd^{2.69}$ hybrid orbital of Ir. More d orbital components are involved in the formation of the Ir–H3 bond in **1** and the Ir–H2 bond in **1′**, leading to the lower orbital energies. In addition, there are unnegligible electron occupancies in the Ir–H σ^* bonds of **1** and **1′**. A larger occupancy appears in the Ir–H1 σ^* bond in **1**, which weakens this bond to a certain extent. As a result of the combined action of these two factors, the Ir–H1 bond of **1** is weaker than the Ir–H3 bond in **1** and the Ir–H2 bond in **1′**. Matsubara found that the protons on a complex have the promotion effect on the nucleophilic attack of the hydride to CO_2.[17] Sakaki and co-workers also disclosed the promotion effect of water molecules.[19] They both suggested that this is because the electrophilicity at the C atom of CO_2 is

enhanced by the hydrogen bonding of the proton or water molecule. In the present work we have shown that which route CO_2 insertion into the Ir–H bond takes, direct addition or migration with the help of the metal center, is determined by the activity of the hydride, and in another word, by the type of the Ir–H bond.

Conclusion

In this study the hydrogenation of CO_2 to formate on the [IrPNPH$_3$] complex has been investigated with density functional theory calculations. Two main pathways for CO_2 insertion into the Ir–H bond were taken into account: (I) Hydride migration to CO_2 with the precoordination of CO_2 to the metal center, and (II) direct addition of hydride to CO_2 via nucleophilic attack. The former involves the cooperation of the metal center. But the results showed that the direct hydride addition to CO_2 is more favorable on this complex. The formation of formate is slightly exothermic by 4.0 kcal mol^{-1} and has a low barrier of 11.0 kcal mol^{-1}, in accord with the experimental observation that the formate formation is facile and reversible. Formate anion can then be eliminated through substitution by an OH group. The deprotonative dearomatization of the pincer ligand leads to the H_2O formation. Finally, H_2 dissociation on this dearomatized complex regenerates the starting active complex. The whole cycle is exothermic by 30.3 kcal mol^{-1} and the rate-limiting step is the regeneration of the active complex, which has an activation barrier of 15.6 kcal mol^{-1}. All these computational results are in good agreement with and give a reasonable explanation to the experimental facts.[11]

The mechanism for the direct addition of hydride to CO_2 and the nature of the Ir–H bonds in the [IrPNPH$_3$] complex have been studied based on MO and NBO analyses. It was shown that the Ir–H bond in the plane of the pyridine moiety and the Ir–H bond vertical to the pyridine moiety are two kinds of metal–hydride bonds. They have distinct bond distances, stretching frequencies, and dissociation energies. The Ir–H bond vertical to the pyridine moiety is formed from the combination of the 1s orbital of hydride with the sd$^{1.73}$ orbital of Ir, whereas the Ir–H bond in the plane of the pyridine moiety is formed from the mixing of the 1s orbital of hydride with the sd$^{2.69}$ orbital of Ir. In addition, the more considerable electron occupancy in the σ^* bond weakens the Ir–H bond vertical to the pyridine moiety. These two factors result in the electrons forming this Ir–H bond having a higher orbital energy and occupying the HOMO. As a result, this HOMO can overlap with the π^* orbital of CO_2 when this hydride attacks CO_2. These results imply that which route the insertion of CO_2 into a metal–hydride bond takes, direct addition or migration with the assistance of the metal center, might be determined by the type of metal–hydride bond. This information would be helpful for the design of other highly active catalysts for the hydrogenation of CO_2.

K.Y. acknowledges Grants-in-Aid (Nos. 18GS0207 and 22245028) for Scientific Research from Japan Society for the Promotion of Science (JSPS) and the Ministry of Education, Culture, Sports, Science and Technology of Japan (MEXT), the Nanotechnology Support Project of MEXT, the MEXT Project of Integrated Research on Chemical Synthesis, the Kyushu University Global COE Project, and CREST of the Japan Science and Technology Cooperation for their support of this work.

Supporting Information

The coordination of CO_2 to the metal center in company with the Ir–P linkage cleavage, the coordination of CO_2 to the metal center after the release of H_2, the optimized geometries of the species in Schemes 6 and 7, and Cartesian coordinates for the optimized geometries of all investigated species. This material is available free of charge on the web at http://www.csj.jp/journals/bcsj/.

References

1 P. G. Jessop, F. Joó, C.-C. Tai, *Coord. Chem. Rev.* **2004**, *248*, 2425.
2 I. Omae, *Catal. Today* **2006**, *115*, 33.
3 T. Sakakura, J.-C. Choi, H. Yasuda, *Chem. Rev.* **2007**, *107*, 2365.
4 M. Aresta, A. Dibenedetto, *Dalton Trans.* **2007**, 2975.
5 K. M. K. Yu, I. Curcic, J. Gabriel, S. C. E. Tsang, *ChemSusChem* **2008**, *1*, 893.
6 W. Leitner, *Angew. Chem., Int. Ed. Engl.* **1995**, *34*, 2207.
7 P. G. Jessop, T. Ikariya, R. Noyori, *Chem. Rev.* **1995**, *95*, 259.
8 a) E. Graf, W. Leitner, *J. Chem. Soc., Chem. Commun.* **1992**, 623. b) J.-C. Tsai, K. M. Nicholas, *J. Am. Chem. Soc.* **1992**, *114*, 5117. c) F. Gassner, W. Leitner, *J. Chem. Soc., Chem. Commun.* **1993**, 1465. d) F. Gassner, E. Dinjus, H. Görls, W. Leitner, *Organometallics* **1996**, *15*, 2078. e) K. Angermund, W. Baumann, E. Dinjus, R. Fornika, H. Görls, M. Kessler, C. Krüger, W. Leitner, F. Lutz, *Chem.—Eur. J.* **1997**, *3*, 755.
9 a) P. G. Jessop, T. Ikariya, R. Noyori, *Nature* **1994**, *368*, 231. b) P. G. Jessop, Y. Hsiao, T. Ikariya, R. Noyori, *J. Am. Chem. Soc.* **1996**, *118*, 344. c) G. Laurenczy, F. Joó, L. Nádasdi, *Inorg. Chem.* **2000**, *39*, 5083. d) C. Yin, Z. Xu, S.-Y. Yang, S. M. Ng, K. Y. Wong, Z. Lin, C. P. Lau, *Organometallics* **2001**, *20*, 1216. e) P. Munshi, A. D. Main, J. C. Linehan, C.-C. Tai, P. G. Jessop, *J. Am. Chem. Soc.* **2002**, *124*, 7963. f) C.-C. Tai, J. Pitts, J. C. Linehan, A. D. Main, P. Munshi, P. G. Jessop, *Inorg. Chem.* **2002**, *41*, 1606. g) A. D. Getty, C.-C. Tai, J. C. Linehan, P. G. Jessop, M. M. Olmstead, A. L. Rheingold, *Organometallics* **2009**, *28*, 5466.
10 a) S. Ogo, R. Kabe, H. Hayashi, R. Harada, S. Fukuzumi, *Dalton Trans.* **2006**, 4657. b) Y. Himeda, N. Onozawa-Komatsuzaki, H. Sugihara, K. Kasuga, *Organometallics* **2007**, *26*, 702. c) M. Erlandsson, V. R. Landaeta, L. Gonsalvi, M. Peruzzini, A. D. Phillips, P. J. Dyson, G. Laurenczy, *Eur. J. Inorg. Chem.* **2008**, 620.
11 R. Tanaka, M. Yamashita, K. Nozaki, *J. Am. Chem. Soc.* **2009**, *131*, 14168.
12 F. Hutschka, A. Dedieu, M. Eichberger, R. Fornika, W. Leitner, *J. Am. Chem. Soc.* **1997**, *119*, 4432.
13 Y. Musashi, S. Sakaki, *J. Chem. Soc., Dalton Trans.* **1998**, 577.
14 Y. Musashi, S. Sakaki, *J. Am. Chem. Soc.* **2000**, *122*, 3867.
15 Y. Musashi, S. Sakaki, *J. Am. Chem. Soc.* **2002**, *124*, 7588.
16 Y. Ohnishi, T. Matsunaga, Y. Nakao, H. Sato, S. Sakaki, *J. Am. Chem. Soc.* **2005**, *127*, 4021.
17 T. Matsubara, *Organometallics* **2001**, *20*, 19.

18 T. Matsubara, K. Hirao, *Organometallics* **2001**, *20*, 5759.
19 Y. Ohnishi, Y. Nakao, H. Sato, S. Sakaki, *Organometallics* **2006**, *25*, 3352.
20 A. Urakawa, F. Jutz, G. Laurenczy, A. Baiker, *Chem.—Eur. J.* **2007**, *13*, 3886.
21 M. S. G. Ahlquist, *J. Mol. Catal. A: Chem.* **2010**, *324*, 3.
22 M. J. Frisch, G. W. Trucks, H. B. Schlegel, G. E. Scuseria, M. A. Robb, J. R. Cheeseman, G. Scalmani, V. Barone, B. Mennucci, G. A. Petersson, H. Nakatsuji, M. Caricato, X. Li, H. P. Hratchian, A. F. Izmaylov, J. Bloino, G. Zheng, J. L. Sonnenberg, M. Hada, M. Ehara, K. Toyota, R. Fukuda, J. Hasegawa, M. Ishida, T. Nakajima, Y. Honda, O. Kitao, H. Nakai, T. Vreven, J. A. Montgomery, Jr., J. E. Peralta, F. Ogliaro, M. Bearpark, J. J. Heyd, E. Brothers, K. N. Kudin, V. N. Staroverov, R. Kobayashi, J. Normand, K. Raghavachari, A. Rendell, J. C. Burant, S. S. Iyengar, J. Tomasi, M. Cossi, N. Rega, J. M. Millam, M. Klene, J. E. Knox, J. B. Cross, V. Bakken, C. Adamo, J. Jaramillo, R. Gomperts, R. E. Stratmann, O. Yazyev, A. J. Austin, R. Cammi, C. Pomelli, J. W. Ochterski, R. L. Martin, K. Morokuma, V. G. Zakrzewski, G. A. Voth, P. Salvador, J. J. Dannenberg, S. Dapprich, A. D. Daniels, O. Farkas, J. B. Foresman, J. V. Ortiz, J. Cioslowski, D. J. Fox, *Gaussian 09 (Revision A.02)*, Gaussian, Inc., Wallingford CT, **2009**.
23 A. D. Becke, *J. Chem. Phys.* **1993**, *98*, 5648.
24 M. Dolg, *Effective Core Potentials* in *Modern Methods and Algorithms of Quantum Chemistry*, ed. by J. Grotendorst, John von Neumann Institute for Computing, Jülich, Germany, **2000**, Vol. 1, pp. 497–508.
25 J. M. L. Martin, A. Sundermann, *J. Chem. Phys.* **2001**, *114*, 3408.
26 T. H. Dunning, Jr., *J. Chem. Phys.* **1989**, *90*, 1007.
27 D. E. Woon, T. H. Dunning, Jr., *J. Chem. Phys.* **1993**, *98*, 1358.
28 a) S. Miertuš, E. Scrocco, J. Tomasi, *Chem. Phys.* **1981**, *55*, 117. b) S. Miertus, J. Tomasi, *Chem. Phys.* **1982**, *65*, 239. c) M. Cossi, V. Barone, R. Cammi, J. Tomasi, *Chem. Phys. Lett.* **1996**, *255*, 327.
29 a) B. Mennucci, J. Tomasi, *J. Chem. Phys.* **1997**, *106*, 5151. b) E. Cancès, B. Mennucci, J. Tomasi, *J. Chem. Phys.* **1997**, *107*, 3032. c) J. Tomasi, B. Mennucci, E. Cancès, *THEOCHEM* **1999**, *464*, 211.
30 E. D. Glendening, J. K. Badenhoop, A. E. Reed, J. E. Carpenter, J. A. Bohmann, C. M. Morales, F. Weinhold, *NBO 5.9*, Theoretical Chemistry Institute, University of Wisconsin, Madison, **2009**.
31 C. Gunanathan, Y. Ben-David, D. Milstein, *Science* **2007**, *317*, 790.
32 H. Grützmacher, *Angew. Chem., Int. Ed.* **2008**, *47*, 1814.
33 J. Zhang, G. Leitus, Y. Ben-David, D. Milstein, *J. Am. Chem. Soc.* **2005**, *127*, 10840.
34 J. Zhang, G. Leitus, Y. Ben-David, D. Milstein, *Angew. Chem., Int. Ed.* **2006**, *45*, 1113.
35 T. Zweifel, J.-V. Naubron, H. Grützmacher, *Angew. Chem., Int. Ed.* **2009**, *48*, 559.
36 J. Li, Y. Shiota, K. Yoshizawa, *J. Am. Chem. Soc.* **2009**, *131*, 13584.